

MgN: a new promising material for spintronic applications

A. Droghetti, N. Baadji and S. Sanvito

School of Physics and CRANN, Trinity College, Dublin 2, Ireland

(Dated: November 20, 2021)

Density functional theory calculations demonstrate that rocksalt MgN is a magnetic material at the verge of half-metallicity, with an electronic structure robust against strong correlations and spin-orbit interaction. Furthermore the calculated heat of formation describes the compound as metastable and suggests that it can be fabricated by tuning the relative Mg and N abundance during growth. Intriguingly the equilibrium lattice constant is close to that of MgO, so that MgN is likely to form as an inclusion during the fabrication of N-doped MgO. We then speculate that the MgO/MgN system may represent a unique materials platform for magnetic tunnel junctions not incorporating any transition metals.

The so called d^0 magnets are currently challenging our conventional understanding of magnetism. These are wide-gap semiconductors and oxide insulators displaying magnetic properties which cannot be ascribed to the presence of partially filled d or f shells¹. Prototypical examples are diamagnetic materials in their well-crystallized bulk form, which present magnetic features when grown as defective thin films. A similar phenomenology is found also in oxides doped with light elements such as N or C^{2,3}. Unfortunately, despite the increasingly large number of reports of d^0 magnets, their typical experimental characterization is often limited to magnetometry with little information about the local electronic structure. The phenomenon thus remains rather obscure. It is characterized by a poor degree of reproducibility and still lacks of a convincing theoretical framework.

Most of the theoretical work to date is based on density functional theory (DFT) utilizing local approximations to the exchange and correlation functional (LDA or GGA). In most of the cases the LDA/GGA, probably correctly, associates the magnetic moment formation to spin-polarized holes residing on either cation vacancies or impurities. In addition the ground state is always predicted ferromagnetic and rather robust. However LDA and GGA usually fail in describing the symmetry details of the wave-function, in particular the polaronic distortion around the magnetic center. Therefore more advanced techniques, including strong electron correlation, appears as necessary^{4,5,6,7}. When applied, these confirm the nature of the magnetic moment formation but almost always predict no long-range magnetic coupling and no ferromagnetism. MgO:N is a prototypical example^{4,5,8,9}. Quantum Monte Carlo calculations for the Anderson-Haldane model indicates the possibility of high temperature ferromagnetism⁹. However DFT calculations using either the LDA+ U or the self-interaction correction (SIC) scheme return impurity levels deep in the gap, holes trapped by polaronic distortions and no room temperature ferromagnetism^{4,5,8}.

Finally another important, but yet scarcely studied, class of d^0 magnets is represented by zincblende (ZB) II-V or II-IV compounds such as CaP, CaAs, CaSb^{10,11,12} or CaC, SrC and BaC¹³. These are weakly covalent solids with either one or two holes per formula unit, and they

are generally predicted to be half-metallic. Intriguingly, although at least for the II-V's the thermodynamical stable phase has the stoichiometric Zn₃P₂-type structure¹⁴, their rocksalt (RS) phase has usually a lower energy than the ZB and it is predicted metastable.

In this work we investigate the magnetic ground state of RS MgN, which was already predicted as half-metal in the ZB phase¹². This is an extremely interesting material because of its structural similarity to the parental MgO, widely used as tunnel barrier in magnetic tunnel junctions¹⁵. We will demonstrate that MgN is a half-metal with negligible spin-orbit interaction and negative formation enthalpy. This means that, although it is not the thermodynamical stable phase, it can be grown as a metastable compound in the form of either thin films or as nanoclusters inside MgO matrices.

Our calculations are performed with a development version of the SIESTA code¹⁶, which includes the atomic self interaction correction (ASIC)¹⁷ and the LDA+ U ¹⁸ schemes. The core electrons are treated with norm-conserving Troullier-Martin pseudopotentials and the valence charge density is expanded over a numerical orbital basis set, including double- ζ and polarized functions¹⁶. The real space grid has an equivalent cutoff larger than 600 Ry, and we sample a minimum of $20 \times 20 \times 20$ k -points in the Brillouin zone. The atomic coordinates are relaxed by conjugate gradient until the forces are smaller than 0.01 eV/Å. For the evaluation of the spin-orbit coupling we have performed full-potential linear augmented plane-waves (FLAPW) calculations¹⁹ with the scheme implemented in FLEUR code²⁰. We use a $12 \times 12 \times 12$ k -point mesh and a plane wave expansion with $k_{\max} = 4$ a.u. A muffin-tin sphere of a radius 2.02 Bohr was taken for both Mg and N with $\ell_{\max}=8$ as cutoff in the ℓ -expansion of the muffin orbitals. Spin-orbit is included by second variation method²¹.

We start our analysis by briefly comparing the ground state of the ZB and RS structures. In table I we report the equilibrium lattice constant, a , the magnetic moment per formula unit, μ , and the magnetic moment formation energy, ΔE_M , for the two structures. ΔE_M is defined as the energy difference per formula unit between the spin-polarized and the non-spin-polarized DFT solution and it is positive when the magnetic state has a lower en-

ergy. Importantly ΔE_M is always substantially larger than zero, demonstrating that the magnetism is robust for both the structures. We also note that our results for the ZB phase are in excellent agreement with previous calculations¹², and that for the RS phase ΔE_M is slightly smaller than that calculated for the same phase of SrN and CaN¹⁴, although it is still well above room temperature.

Structure	LDA			GGA		
	a	μ	ΔE_M	a	μ	ΔE_M
ZB	4.73	1.0	157	4.83	1.0	180
RS	4.34	1.0	60	4.44	1.0	95

TABLE I: Equilibrium lattice constant a (in Å), magnetic moment per formula unit μ (in μ_B) and ΔE_M (in meV) for ZB and RS MgN.

Next we discuss in details the electronic structure of RS MgN. The GGA bandstructure calculated at the equilibrium lattice constant of 4.44 Å and displayed in Fig. 1, clearly reveals the half-metallic character of MgN with a direct gap of 5 eV at the Γ point in the minority spin-channel. This is different from the bandstructure for RS CaN where the gap is indirect with the conduction band minimum located at X¹⁴. The differences between CaN

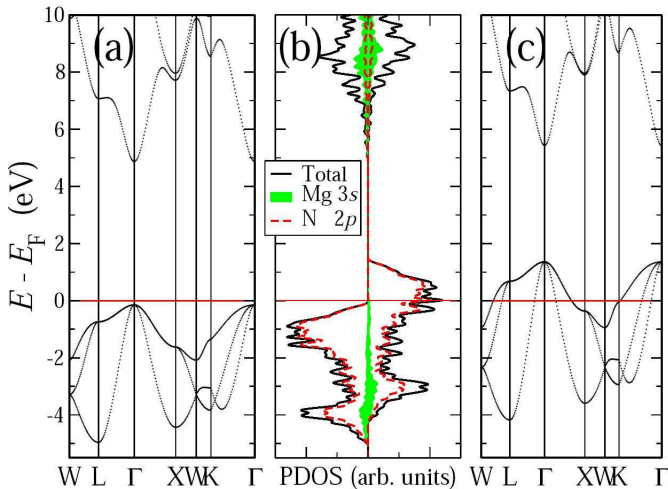


FIG. 1: GGA band structure for RS MgN calculated at the equilibrium lattice constant of 4.44 Å: panel (a) majority spin, panel (c) minority. The horizontal red line denotes the position of Fermi level. In panel (b) we report the associated total density of states (black solid line) and density of states projected over the N-2p (red dashed line) and Mg-3s (green shadowed area)

and MgN can be understood by looking at the orbital projected density of states (PDOS) presented in Fig. 1(b). In the case of MgN the N 3d levels are unbound and they only weakly mix with the Mg 3s, which form the conduc-

tion band. In contrast the empty Ca 3d levels provide the dominant contribution to the conduction band of CaN, shifting the band minimum to the X point. Furthermore their hybridization with the N 2p orbitals forming the valence band is rather strong and result in the CaN valence band being considerably more flat than that of MgN. In summary the main difference between RS MgN and CaN is in the different role played by the cation 3d orbitals. Interestingly it was suggested¹⁰ that the contribution of the Ca-d level in Ca pnictides is fundamental to promote the half metallicity. Later such a claim was challenged by the statement that the magnetic moment formation in II-V compounds is driven by the strong atomic character of the anions¹⁴. MgN demonstrates that both of the arguments are partially correct. Indeed the ionicity in SrN, CaN and MgN is able to localize the hole on N leading to the formation of the magnetic moment. However the hybridization with the d shell of the cation increases the flatness of the top of valence band causing an enhancement of ΔE_M .

We then investigate the robustness of the half-metallic ground state with respect to compression, spin-fluctuations, choice of exchange and correlation functional and spin-orbit interaction. In figure 2 we report the magnetic moment as a function of the lattice constant as calculated with GGA (the LDA results are rather similar). Importantly we note that there is a broad range of lattice constants for which MgN preserves the half-metal moment of 1 μ_B . For a smaller than 4.3 Å the moment becomes fractional and the material turns into a standard ferromagnet, until it finally becomes non-spin-polarized for a massive compressive pressure ($a < 3.0$ Å). Interestingly at the MgO lattice constant (4.21 Å) the magnetic state of MgN is still extremely close to that of a half-metal. This is a tantalizing feature suggesting that, should MgN be made in MgO, it will be an efficient spin polarizer/analyzer in transition metal free tunnel junctions. Finally note that for a largely expanded lattice parameter the moment reaches the value of 3 μ_B expected from isolated N ions.

Spin excitations and the possible effects arising from strong correlations are analyzed next. In particular we calculate the total energy difference per formula unit between the ferromagnetic and either the type-I ($\Delta E_{\uparrow\uparrow-\uparrow\downarrow}^I$) and type-II ($\Delta E_{\uparrow\uparrow-\uparrow\downarrow}^{II}$) antiferromagnetic state. These are both characterized by a planar ferromagnetic alignment with antiparallel orientation between planes, either along the (001) (type-I) or (111) (type-II) direction. At the equilibrium lattice constant we find $\Delta E_{\uparrow\uparrow-\uparrow\downarrow}^I = 52$ meV ($\Delta E_{\uparrow\uparrow-\uparrow\downarrow}^I = 67$ meV) and for $\Delta E_{\uparrow\uparrow-\uparrow\downarrow}^{II} = 53$ meV ($\Delta E_{\uparrow\uparrow-\uparrow\downarrow}^{II} = 68$ meV) for LDA (GGA). These are rather similar to ΔE_M indicating that in MgN Stoner and spin-wave excitations compete.

It is then interesting to investigate how the moment formation and the energetic of the spin-excitations change when electron correlation is added to the electronic structure. This is investigated with the LDA+U scheme applied to the N-2p shell as a function of U (J

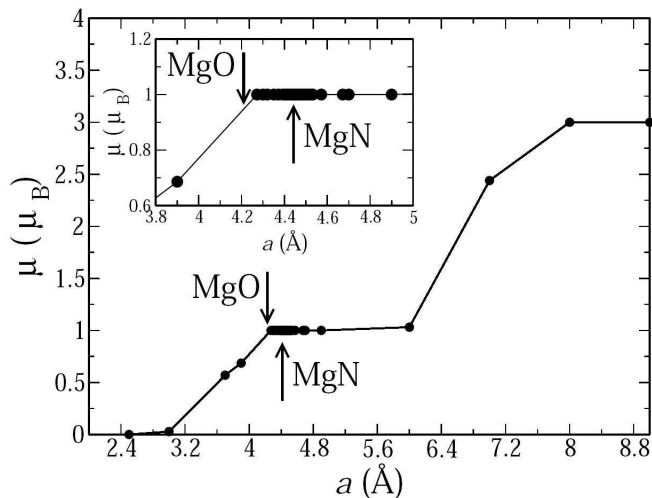


FIG. 2: Magnetic moment μ per formula unit as a function of the lattice constant for RS MgN as calculated with GGA. The inset shows a zoom at around the GGA equilibrium value of 4.44 Å. The arrows indicate the experimental MgO and the GGA-calculated MgN lattice constants.

is kept at zero). Our results are reported in table II. As expected the addition of on-site correlation to the N-2*p* shell downshifts its center of mass effectively opening the band-gap in both the spin-bands. This is associated to a considerable strengthening of the ferromagnetic interaction, with both $\Delta E_{\uparrow\uparrow-\uparrow\downarrow}^I$ and $\Delta E_{\uparrow\uparrow-\uparrow\downarrow}^{II}$ increasing monotonically with U . In the table we also report the exchange split, ΔE_{ex} , which is the energy difference between the top of the majority and minority valence bands for the ferromagnetic ground state at its equilibrium lattice constant. We note that also ΔE_{ex} increases with U with an almost perfectly linear dependence. Finally we find that the critical lattice constant for the half-metallicity gets progressively reduced as U gets larger, while the equilibrium lattice parameter seems to be only marginally affected by U .

The promotion of the magnetic stability in RS MgN with increasing U can be understood by using the DFT version of the standard Stoner argument applied to the LDA+ U functional²². In fact, in the limit of uniform occupancy of the strongly correlated shell (N-2*p* in our case), one expects the Stoner parameter to increase linearly with U . This may, of course, be compensated by a reduction of the density of states at the Fermi energy (E_F), resulting in an overall reduction of the magnetic interaction. In the case of RS MgN, however, both the band-width and the curvature of the bands near E_F change little with U , since such a valence band has a pure N-2*p* character. As a consequence we find an almost perfect linear relation between the exchange split ΔE_{ex} and U , which confirms the Stoner nature of the ferromagnetism in MgN. This leads us to conclude that the addition of strong correlations through an on-site Coulomb repulsion enhances the stability of the half-metal charac-

ter of RS MgN.

U	a_c	E_{gap}	ΔE_{ex}	$\Delta E_{\uparrow\uparrow-\uparrow\downarrow}^I$	$\Delta E_{\uparrow\uparrow-\uparrow\downarrow}^{II}$
(eV)	(Å)	(eV)	(eV)	(meV)	(meV)
GGA	4.3	5.0	1.51	52	53
2	3.8	6.19	2.15	95	96
3	3.6	6.40	2.48	172	156
4	3.5	6.75	2.94	267	251
5	3.4	7.16	3.30	344	338
6	3.4	7.40	3.77	395	392
7	3.3	8.09	4.23	443	428
8	3.2	8.17	4.68	472	463
ASIC	3.6	7.51	4.24	184	175

TABLE II: Critical lattice constant for the half-metallicity, a_c , minority spin bandgap, E_{gap} , exchange split ΔE_{ex} , and ferromagnetic to antiferromagnetic total energy difference $\Delta E_{\uparrow\uparrow-\uparrow\downarrow}^I$ and $\Delta E_{\uparrow\uparrow-\uparrow\downarrow}^{II}$, as a function of the on-site Coulomb interaction U .

In table II we also report results obtained with the ASIC method, which was proved to yield an accurate MgO bandgap and the proper polaronic distortion in diluted d^0 magnets⁴. The ASIC returns both a critical lattice constant for the half-metallicity and magnetic energies similar to those calculated with LDA+ U and $U \sim 3$ eV. However the bandgap and Δ_{ex} are considerably larger and compatible with $U = 6$ eV. Although it is difficult to make any strong quantitative statement, because the mixed success of ASIC in predicting exchange constants²³, the result further confirms that the half-metallic state of MgN is strong with respect to strong electron correlation.

Finally we investigate the effect of the spin-orbit coupling on the electronic structure of MgN. In general spin-orbit interaction always destroys the half-metallicity of a magnet by mixing the two spin channels. Our calculations however show that the spin-orbit coupling constant between the spin and the orbital angular momentum is only of the order of 10 meV. Furthermore, the MgN highly symmetric cubic environment quenches the angular magnetic moment, which is only $7 \times 10^{-5} \mu_B$ for Mg and $9.8 \times 10^{-4} \mu_B$ for N. It is then not surprising that the spin polarization remains 100 % even after the spin-orbit interaction is accounted for, i.e. the half-metallicity is preserved.

After having discussed the electronic properties of MgN we now turn our attention to analyzing the structural stability of the RS structure. First we compare the total energy per cell of volume of four different crystal structures, likely candidates for MgN, namely wurzite, ZB, NiAs-type (space group $P6_3/mmc$) and RS. As shown in figure 3 the RS structure presents both the lower total energy and smaller equilibrium volume of all the crystals investigated, indicating that it is the most thermodynamic favorable. This however still does not mean that MgN can be made. In fact one has to compare the

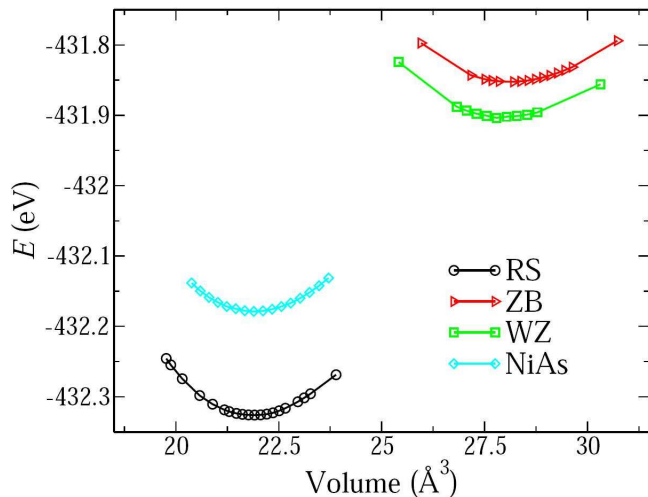


FIG. 3: (Color on line) Total energy as a function of the volume per formula unit for MgN with wurtzite (WZ), zincblende (ZB), NiAs and rock-salt (RS) crystal structure.

stability of RS MgN with that of its stoichiometric stable form Mg_3N_2 , i.e. one has to demonstrate that the heat of formation for RS MgN, ΔH_{MgN} , is comparable to that of Mg_3N_2 , $\Delta H_{\text{Mg}_3\text{N}_2}$.

Mg_3N_2 is a non-magnetic semiconductor with an experimental band gap of 2.8 eV²⁵ and with the tetragonal bixbyite crystal structure. The experimental lattice constant is 9.953 Å²⁴ while our calculations return values of 9.85 Å (LDA) and 10.01 Å (GGA). These are both within 1% of the experimental reported values. The heats of formation can be written as

$$\Delta H_{\text{Mg}_3\text{N}_2} = 1/5 [1/8 E_{\text{Mg}_3\text{N}_2} - (3/2 E_{\text{Mg}} + E_{\text{N}_2})], \quad (1)$$

$$\Delta H_{\text{MgN}} = 1/2 [E_{\text{MgN}} - 1/2 (E_{\text{Mg}} + E_{\text{N}_2})], \quad (2)$$

where E refers to the total energy and Mg is assumed in its *hcp* metallic phase. We calculate $\Delta H_{\text{Mg}_3\text{N}_2} = -1.44$ eV/atom ($\Delta H_{\text{Mg}_3\text{N}_2} = -1.16$ eV/atom) and $\Delta H_{\text{MgN}} = -0.91$ eV/atom ($\Delta H_{\text{MgN}} = -0.59$ eV/atom) with LDA (GGA). Although, as expected Mg_3N_2 has a lower heat of formation and forms at equilibrium, RS MgN also has a negative ΔH . This means that it is a thermodynamic stable compound, and hence that RS MgN is metastable. We then speculate that the relative abundance of N and Mg during the growth process, in addition to the choice of substrate, can drive the formation of either Mg_3N_2 or MgN. Intriguingly MgO appears as an ideal substrate for the growth of MgN but metals with bcc lattice structure are equally tantalizing. Among them we mention V, Mo and W.

In conclusion we investigated the electronic and structural properties of rocksalt MgN. This was found to be at the verge of half-metallicity in LDA and GGA and completely half-metallic as soon as some electron correlation is included. The half-metallicity is then robust with compression and spin-orbit interaction. Furthermore we have then demonstrated that the RS phase is the most stable among the various possible MgN phases. Its heat of formation is negative, but smaller than that of Mg_3N_2 , suggesting that MgN can be possibly made by tuning the relative Mg and N abundances during growth and the substrate crystal structure.

This work is sponsored by Science Foundation of Ireland (07/RFP/MASF238) and by the EU 6th Framework (SpiDME project). Computational resources have been provided by the HEA IITAC project managed by the Trinity Center for High Performance Computing and by ICHEC.

-
- ¹ J.M.D. Coey, Solid State Sci., **7**, 660 (2005).
² H. Pan et al., Phys. Rev. Lett. **99**, 127201 (2007).
³ S. Zhou et al., Appl. Phys. Lett., **93**, 232507 (2008).
⁴ A. Droghetti, C. D. Pemmaraju and S. Sanvito, Phys. Rev. B, **78**, 140404(R) (2008).
⁵ V. Pardo and W. E. Pickett, Phys. Rev. B, **78**, 134427 (2008).
⁶ I.S. Elfimov et al., Phys. Rev. Lett. **98**, 137202 (2007).
⁷ S. Lany and A. Zunger, arXiv:0905.0018.
⁸ A. Droghetti and S. Sanvito, arXiv:0902.4471.
⁹ B. Gu, N. Bulut, T. Ziman and S. Maekawa, Phys. Rev. B, **79**, 024407 (2009).
¹⁰ K. Kusakabe, M. Geshi, H. Tsukamoto and N. Suzuki, J. Phys.:Condens. Matter **16**, 5639 (2004).
¹¹ O. Volnianska, P. Jakubas and P. Bogusławski, J. Alloys Compd., **423**, 191 (2006).
¹² M. Sieberer, J. Redinger, S. Khmelevskiy and P. Mohn, Phys. Rev. B **73**, 024404 (2006).
¹³ G.Y. Gao et al., Phys. Rev. B, **75** 174442 (2007).
¹⁴ O. Volnianska and P. Bogusławski, Phys. Rev. B, **75**, 224418 (2007).
¹⁵ S.S.P. Parkin et al., Nature Mater. **3**, 862 (2004).
¹⁶ J. M. Soler et al., J. Phys.: Condens. Matter **14**, 2745(2002).
¹⁷ C. D. Pemmaraju, T. Archer, D. Sanchez-Portal and S. Sanvito, Phys. Rev. B **75**, 045101 (2007).
¹⁸ T. Archer, R. Hanafin and S. Sanvito, Phys. Rev. B **78**, 014431 (2008).
¹⁹ M. Weinert, E. Wimmer, and A.J. Freeman, Phys. Rev. B **26**, 4571 (1982).
²⁰ <http://www.flapw.de>
²¹ C. Li, A.J. Freeman, H.J.F. Jansen and C.L. Fu, Phys. Rev. B **42** 5433 (1990).
²² A.G. Petukhov, I.I. Mazin, L. Chioncel and A.I. Lichtenstein, Phys. Rev. B **67**, 153106 (2003).
²³ A. Akande and S. Sanvito, J. Chem. Phys. **127**, 034112 (2207).
²⁴ D.E. Partin, D.J. Williams and M. O’Keeffe, J. Solid State

Chem. **132**, 56 (1997).
²⁵ C.M. Fang, R.A. de Groot, R.J. Bruls, H.T. Hintzen and

G. de With, J. Phys.:Condens. Matter **11**, 4833 (1999).